World Academy of Science, Engineering and Technology
International Journal of Electronics and Communication Engineering
Vol:18, No:6, 2024

High-Power Amplifier Pre-distorter Based on Neural Networks for 5G Satellite Communications

Abdelhamid Louliej, Younes Jabrane

***Abstract*—**Satellites are becoming indispensable assets to fifth-generation (5G) new radio architecture, complementing wireless and terrestrial communication links. The combination of satellites and 5G architecture allows consumers to access all next-generation services anytime, anywhere, including scenarios, like traveling to remote areas (without coverage). Nevertheless, this solution faces several challenges, such as a significant propagation delay, Doppler frequency shift, and high Peak-to-Average Power Ratio (PAPR), causing signal distortion due to the non-linear saturation of the High-Power Amplifier (HPA). To compensate for HPA non-linearity in 5G satellite transmission, an efficient pre-distorter scheme using Neural Networks (NN) is proposed. To assess the proposed NN pre-distorter, two types of HPA were investigated: Travelling Wave Tube Amplifier (TWTA) and Solid-State Power Amplifier (SSPA). The results show that the NN pre-distorter design presents an Error Vector Magnitude (EVM) improvement by 95.26%. Normalized Mean Square Error (NMSE) and Adjacent Channel Power Ratio (ACPR) were reduced by -43,66 dB and 24.56 dBm, respectively. Moreover, the system suffers no degradation of the Bit Error Rate (BER) for TWTA and SSPA amplifiers.

***Keywords*—**Satellites, 5G, Neural Networks, High-Power Amplifier, Travelling Wave Tube Amplifier, Solid-State Power Amplifier, EVM, NMSE, ACPR.

I. Introduction

THE next generations of wireless communication systems are expected to support more significant numbers of smart devices and connected sensors, requiring better quality of service (QoS) and quality of experience (QoE). To meet these requirements, the fifth-generation (5G) aims to provide greater capacity, more data rate, less latency, and better energy efficiency for low-power devices, as well as large numbers of connected devices compared to 4G systems [1]. All these improved factors make emerging wireless systems integration easier, such as broadband systems and the Internet of Things (IoT) [2]. Also, 5G is required to provide connectivity to emerging applications, such as industrial automation, connected car, online healthcare, smart city, smart home, smart grid, and high-speed transportation such as trains, planes, and drones. Satellites must be deployed to ensure affordable and reliable coverage anytime, anywhere in the world. Indeed, satellite communication is becoming essential in the 5G ecosystem, complementing wireless and fixed terrestrial communications [3]. In light of this, the Third Generation Partnership Project (3GPP) has identified three scenarios in which satellites can play a role [4]-[7]:

1) Ensure 5G coverage in areas not served by the terrestrial network (e.g. remote and rural areas).
2) Improve the continuity of 5G services for IoT devices or on-board of high-speed transport platforms.
3) Make the 5G network more scalable by providing an efficient multicast and broadcast resource for data delivery to the network edge.

To amplify satellite signals, Travelling Wave Tube (TWTA) and Solid-State Power (SSPA) amplifiers are the most reliable and efficient choices [8]. However, these amplifiers are highly non-linear, therefore a large back-off is required to avoid signal distortion. As a result, HPA efficiency is significantly reduced [9]. To achieve a large back-off, several techniques were proposed to decrease the input signal PAPR [10], [11]. However, the non-linearity of HPA still provokes a significant distortion, compromising the system's performance. An input signal pre-distortion is required to overcome this drawback, allowing HPA nonlinearity compensation. In this paper, we developed a simple pre-distorter architecture based on NN for a 5G satellite communication system. The solution is tested on TWTA and SSPA amplifiers.

The remainder of this paper is organized as follows. Sections II and III describe UFMC 5G waveform and HPA models. Section IV presents NN models for HPA pre-distortion. Results are detailed in Section V. Finally, Section VI summarizes the conclusion of the paper.

II. UFMC 5G Waveform

Even though Orthogonal Frequency Division Multiplexing (OFDM) was widely deployed in previous wireless communication standards, it still shows some drawbacks that can be summarized as follow. Firstly, the frequency leakage is caused by its rectangular pulse shape. Secondly, the Spectral Efficiency (SE) loss is due to Cyclic Prefix (CP) insertion. Finally, a high Doppler frequency shift affects the inter-symbol and inter-carrier interference, destroying the orthogonality between subcarriers. Several alternative waveforms have been studied in the literature to overcome these limitations. In this paper, we focus on Universal Filtered Multi-Carrier (UFMC) waveform [12], [13]. As its name implies, UFMC is a filtered multicarrier modulation designed in a way to reduce out-of-band emission (OBE).

UFMC applies filtering to a group of subcarriers leading to a lower Adjacent Channel Leakage Ratio (ACLR). UFMC output can be transformed into a classic OFDM waveform by modifying the filter parameters. As shown in Fig. 1, the UFMC

Abdelhamid Louliej is with LPMC Lab, Ibn Zohr University, Agadir 80000, Morocco (e-mail: a.louliej@uca.ma).

Younes Jabrane is with MSC Lab, Cadi Ayyad University, Marrakech 40000, Morocco (e-mail: a.louliej@uca.ac.ma).

transmitter is composed of B sub-bands. In each one, four operations are applied: Quadrature Amplitude Modulation (QAM), serial to parallel, Inverse Fast Fourier Transform (IFFT), and filtering. All B sub-bands are mixed to form the final UFMC waveform x_k expressed as [12], [13]:

$$x_k = \sum_{i=1}^{B} C_{i,K} F_{i,k} S_{i,k} \quad (1)$$

S_i is modulated data vector containing n_i QAM complex values in the i_{th} sub-band, F_i is S_i symbols transformed to time-domain by IFFT matrix of size $N_{FFT} \times n_i$, C_i is F_i filtered with a Dolph-Chebyshev shaping filter of length L, and x_k is the UFMC time-domain transmit vector of length $N_{FFT} + L - 1$.

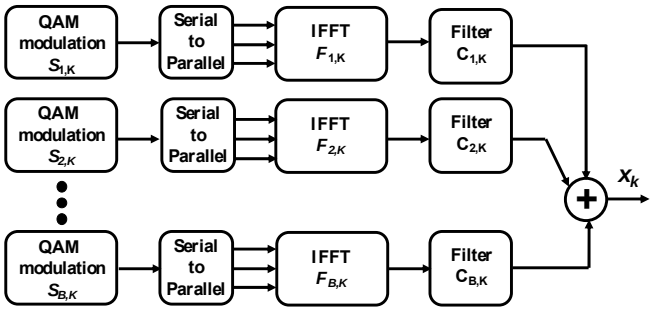

Fig. 1 UFMC transmitter

Knowing that the UFMC modulates each data block B, at the same time, the receiver can directly demodulate the UFMC signal by a simple OFDM demodulator. Note that it is necessary to add zero padding before applying OFDM demodulator with a 2 N_{FFT} points FFT which imposes a factor 2 decimation to recover the data.

III. High-Power Amplifier Models

TWTA and SSPA are the principal and efficient amplifiers for space radio-frequency communications with reduced size, cost, and improved thermal performance. TWTA and SSPA are more adapted for higher frequencies at a significant transmitting power. To reflect the behavior of TWTA and SSPA, two models are used, Saleh and Rapp [14]. For the two models, the output $y_k(t)$ of the nonlinear amplifier can be written as follows:

$$y_k(t) = AM(|x_k(t)|)e^{j[PM(|x_k(t)|)+\phi(x_k(t))]} \quad (2)$$

AM and PM are the magnitude (AM/AM) and phase (AM/PM) transfer functions, while $|x_k(t)|$ and $\phi(x_k(t))$ are input signal magnitude and phase.

A. TWTA's Saleh Model

As previously mentioned, TWTA transfer functions AM and PM can be described according to Saleh's model. Thus, these two functions can be written as follows [14]:

$$AM(|x_k(t)|) = \frac{\alpha_{\|}|x_k(t)|}{(1+\beta_{\|}|x_k(t)|^2)} \quad (3)$$

$$PM(|x_k(t)|) = \frac{\alpha_{PM}|x_k(t)|^2}{(1+\beta_{PM}|x_k(t)|^2)} \quad (4)$$

All parameters $\alpha_{\|}$, $\beta_{\|}$, α_{PM}, and β_{PM} are adjusted to match TWTA's characteristics.

B. SSPA's Rapp Model

In the case of the SSPA, the Rapp model is instead used. The two transfer functions are replaced by the following [14]:

$$AM(|x_k(t)|) = g\frac{|x_k(t)|}{\left(1+\left(\frac{g|x_k(t)|}{A_{sat}}\right)^{2s}\right)^{\frac{1}{2s}}} \quad (5)$$

$$PM(|x_k(t)|) = g\frac{\alpha|x_k(t)|^{c_1}}{\left(1+\left(\frac{|x_k(t)|}{\beta}\right)^{c_2}\right)} \quad (6)$$

g is the signal gain, s is the smoothness factor, A_{sat} is the saturation level, and the rest of the parameters α, β, c_1, and c_2 are adjusted to meet the amplifier characteristics.

In both HPA models, Input Back Off (IBO) is used to determine the required power levels for amplification in its linear region. IBO can be described as:

$$IBO = 10\log_{10}\frac{P_{sat}}{P_{avg}} \quad (7)$$

P_{sat} is the input power saturation, and P_{avg} is the input power average. The behavior of the two HPA models is summarized in Fig. 2.

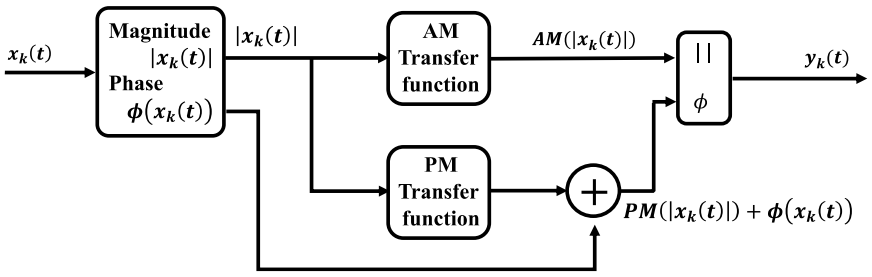

Fig. 2 HPA's operating principle

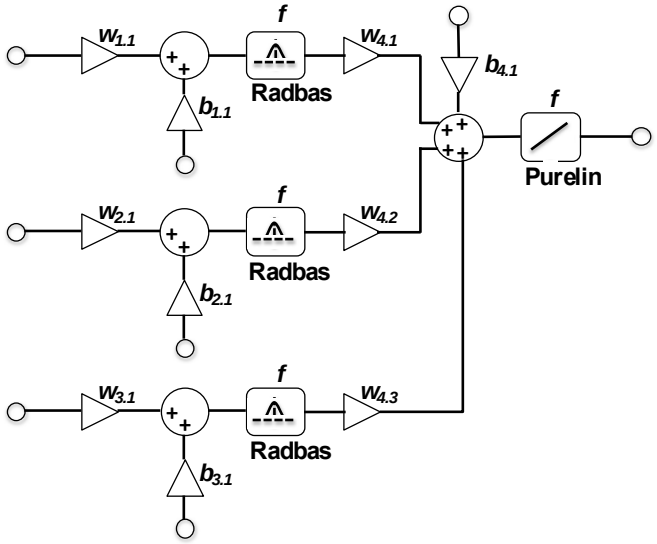

Fig. 3 MLPs pre-distorter architecture

IV. Neural Networks Pre-Distorter Models

Artificial neural networks are made up of simple elements operating in parallel. The interconnection between all of these elements defines the desired behavior. The architecture of an artificial neuron is inspired by biological nervous systems existing in nature, especially those of the human brain. The perceptron is the most common artificial neuron [15]. The perceptron input data $E_{i,n}$ are multiplied by ponderation weights $W_{i,n}$. The results of these ponderations are summed with a bias b to form the activation function input [16]. The activation function is used to determine the output state of an artificial neuron. One of the most used NN architectures is Multilayer Perceptron (MLP). MLP is a fully connected network to classify data that cannot be separated linearly [16]. The NN pre-distorter proposed in this article is an MLP allowing compensation of amplitude (AM) and phase (PM) distortions by adding an inverse nonlinearity to the input signal. By applying inverse nonlinearity, the HPA input can be written as follows:

$$x'_k(t) = AM^{-1}(|x_k(t)|)e^{j[PM^{-1}(|x_k(t)|)+\phi(x_k(t))]} \quad (8)$$

AM^{-1} and PM^{-1} are amplitude and phase inverse functions. Two MLP pre-distorters, NN AM/AM and NN AM/PM, are proposed to synthesize inverse functions. Each MLP consists of the following layers (Fig. 3):

1) The input layer: receives the input signal magnitude $|x_k(t)|$.
2) The hidden layer: includes three perceptrons with a radial basis activation function (Radbas).
3) The output layer: contains a single perceptron with a linear activation function (Purelin).

To determine the values of the weighting coefficients, each MLP is offline trained using the Levenberg-Marquardt algorithm [17]. The offline training is stopped if the mean squared error (MSE) [18] or the number of epochs is reached. The offline training process can be achieved by following steps:

1) Decompose the UFMC signal $x_k(t)$ into magnitude $|x_k(t)|$ and phase angle $\phi(x_k(t))$.
2) Put the magnitude $|x_k(t)|$ through HPA AM and PM transfer functions to obtain $AM(|x_k(t)|)$ and $PM(|x_k(t)|)$ outputs.
3) Synthesize the AM^{-1} pre-distorter function by training the first MPL (NN AM/AM) using the extracted magnitudes $|x_k(t)|$ and $AM(|x_k(t)|)$.
4) Synthesize the PM^{-1} pre-distorter function by training the second MLP (NN AM/AM) using the magnitudes $|x_k(t)|$ and the difference between HPA AM/PM output and phase angle of input signal $PM(|x_k(t)|) - \phi(x_k(t))$.

Note that for the NN AM/AM model, $AM(|x_k(t)|)$ is the training input, and $|x_k(t)|$ is the target. While for the NN AM/PM model, $|x_k(t)|$ is the input, and $PM(|x_k(t)|) - \phi(x_k(t))$ is the training target. The offline training process is depicted in Fig. 4.

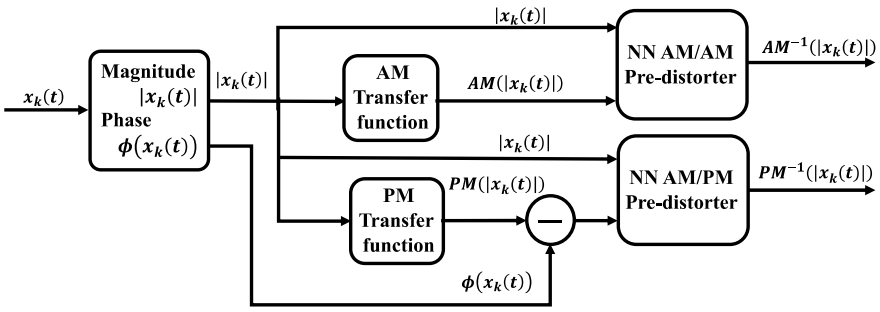

Fig. 4 Offline training process

Following offline training, both MLP models are implemented before HPA and are able to pre-distort the input signal adequately, as shown in Fig. 5.

V. Simulation and Results

To train the NN pre-distortion models, all parameters are set as follows: MSE = 1E-6, number epochs = 1000, and number of UFMC symbols = 1000. Fig. 6 illustrates the NN AM/AM and NN AM/PM training results using TWTA and SSPA transfer functions.

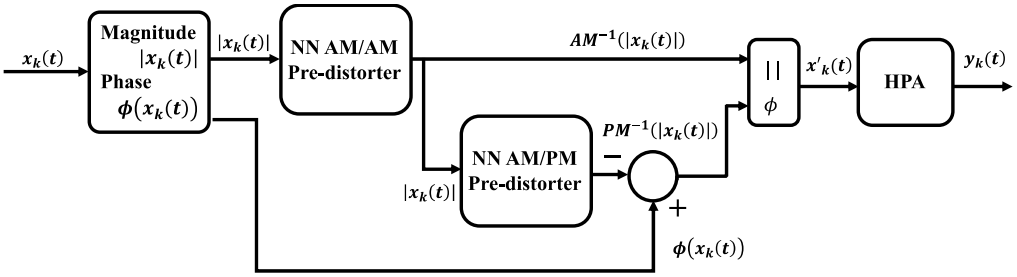

Fig. 5 MLP pre-distorter implementation

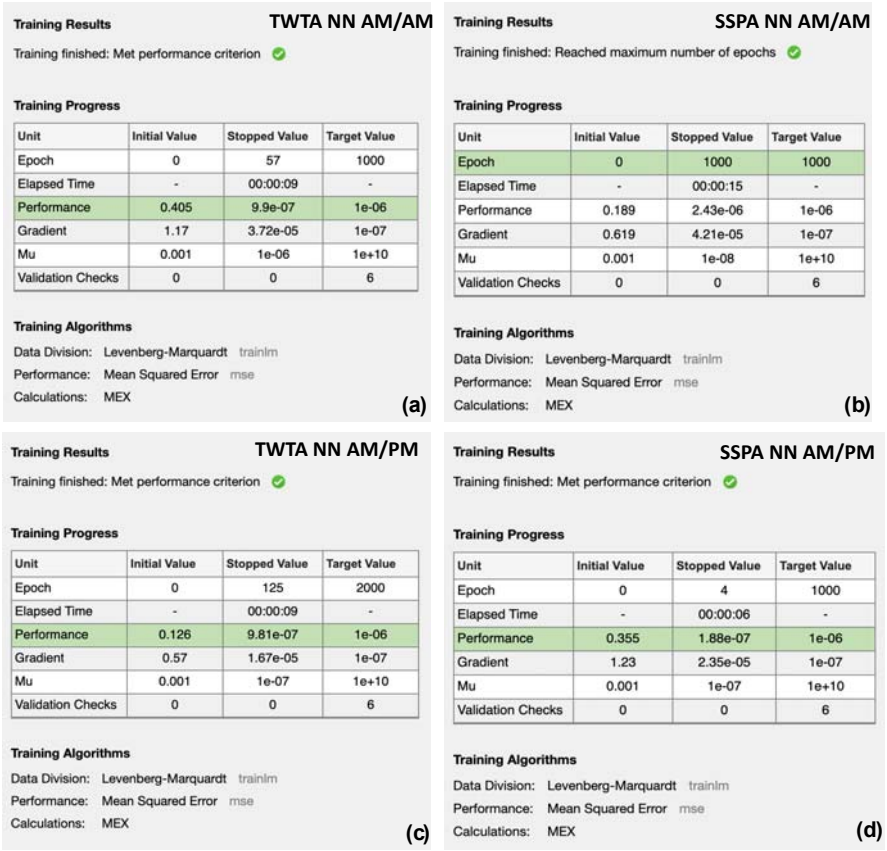

Fig. 6 MLP pre-distorter training results

As shown in Figs. 6 (a) and (c), in the case of the TWTA amplifier, the NN AM/AM and NN AM/PM training stopped at MSE equal to 9.9e-7 and 9.81e-7, respectively. In the case of SSPA (Figs. 6 (b) and (d)), the training stopped for the two models at the 1000th epoch, and MSE = 1.88e-7, respectively.

To evaluate trained NN pre-distorter models, the following performance metrics are adopted:

A. Normalized Mean Square Error

To evaluate the pre-distorter model's performance behavior, NMSE is commonly used [19]. It is often expressed in decibels, and defined according to (9):

$$NMSE(dB) = \frac{\sum_{i=1}^{N}|x_k - y_k|^2}{\sum_{i=1}^{N}|x_k|^2} \quad (9)$$

where x_k is the UFMC symbol, N is its length, and y_k can be either the output signal of the HPA or the NN pre-distorter output (y'_k).

B. Error Vector Magnitude

EVM is a common way to assess the quality of digitally modulated signals [20]. EVM measures the amplitude and the phase errors between transmitted and received modulation constellations. Fig. 7 shows the inflected EVM by TWTA (constellation distortion) and its reduction by NN pre-distorter. The average EMV is defined as:

$$EVM = \sqrt{\frac{\sum_{j=1}^{N_p}\sum_{i=1}^{N_c}(R_{i,j} - S_{i,j})}{N_c N_p}} \quad (10)$$

N_p is the number of frames, N_c is the number of QAM carriers, $R_{i,j}$ is the received QAM symbol, and $S_{i,j}$ is the transmitted

QAM symbol.

Table I summarizes the NMSE and EVM obtained values with and without NN pre-distorters models.

TABLE I
NMSE AND EVM RESULTS

HPA type	TWTA		SSPA	
Performance metric	EVM %	NMSE (dB)	EVM %	NMSE (dB)
Without NN pre-distorter	85.562	-1.3066	96.137	3.4532
With NN pre-distorter	0.5419	-44.97	0.87367	-39.149

Using the NN pre-distorter, the EVM in the case of TWTA and SSPA was reduced by 85% and 95.26%, respectively. NMSE was reduced by -43,66 dB and -42,6 dB.

C. Adjacent Channel Power Ratio

The ACPR refers to the ratio of the primary frequency channel transmitted power to that of the adjacent frequency channels [21]. Indeed, ACPR ensures that the transmitted signal does not interfere with nearby frequency bands. ACPR can be measured as described in (10). Fig. 8 shows the measured ACPR in the case of TWTA (a) and SSPA (b) with and without NN pre-distorter. Results show an ACPR reduction of -24.56 dBm and -22.9 dBm.

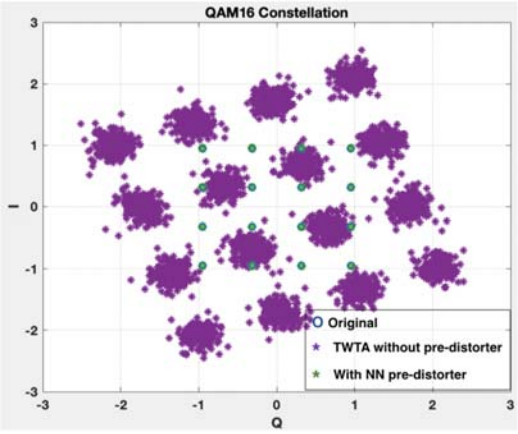

Fig. 7 TWTA QAM16 constellation with and without NN pre-distorter

$$ACPR = \frac{Adjacent\ channels\ Power}{Main\ channelPower} \quad (11)$$

D. Bit Error Rate

To ensure the integrity of received data using the proposed pre-distorter, a BER simulation is carried out with Additive white Gaussian noise (AWGN) channel and different QAM states (4,16 and 64). As shown in Figs. 9 and 10, the proposed NN pre-distorter performance does not undergo any degradation for TWTA and SSPA Amplifiers.

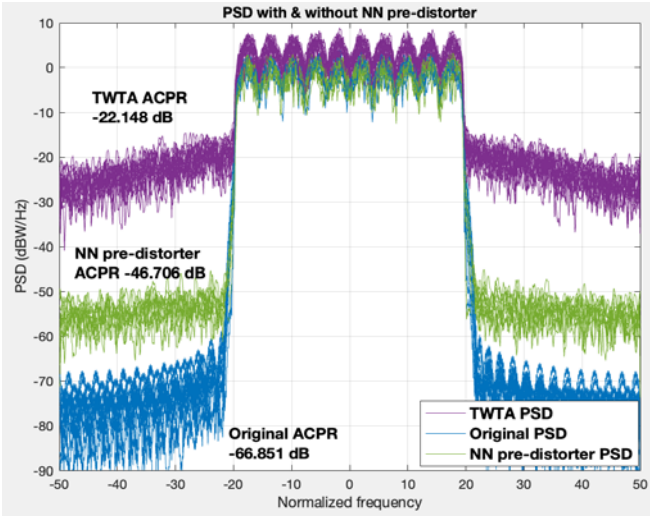

Fig. 8 PSD and ACPR measurements with and without NN pre-distorter

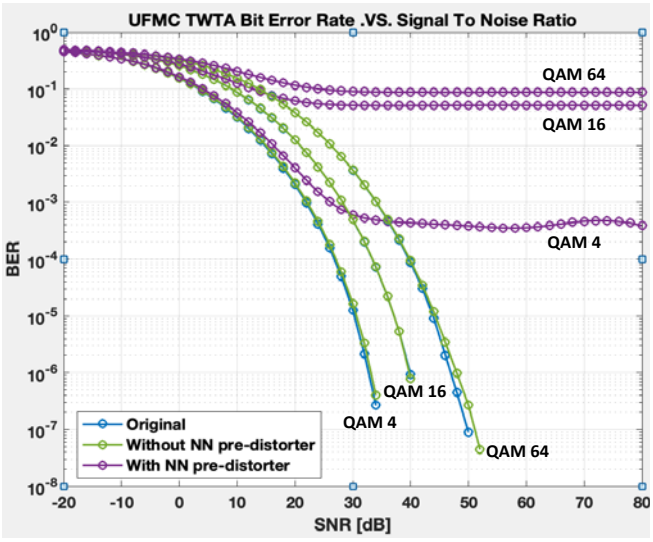

Fig. 9 TWTA BER without and with NN pre-distorter

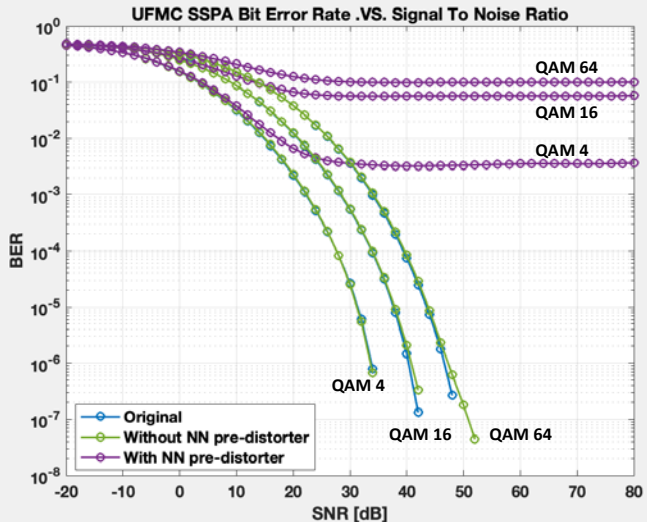

Fig. 10 SSPA BER without and with NN pre-distorter

VI. Conclusion

In this paper, an efficient NN pre-distorter has been designed and tested on UFMC waveform using two types of satellite HPA, TWTA and SSPA. Four metrics were used to assess the performance of the proposed solution. EVM, NMSE, and ACPR were reduced by 95.26 %, -43,66 dB, and -24.56 dBm, respectively. To ensure the integrity of the data received following the application of the NN pre-distorter, the modulation constellation and BER have been successfully plotted. The results show that the system does not undergo any BER degradation for both TWTA and SSPA. For future works, this proposal can be used on other 5G waveforms.

References

[1] A. Ghosh, A. Maeder, M. Baker and D. Chandramouli, "5G Evolution: A View on 5G Cellular Technology Beyond 3GPP Release 15," in IEEE Access, vol. 7, pp. 127639-127651, 2019.

[2] L. Chettri and R. Bera, "A Comprehensive Survey on Internet of Things (IoT) Toward 5G Wireless Systems," in IEEE Internet of Things Journal, vol. 7, no. 1, pp. 16-32, Jan. 2020.

[3] J. Li, D. Wang, L. Liu, B. Wang and C. Sun, "Satellite Ephemeris Broadcasting Architecture for 5G Integrated LEO Satellite Internet," 2022 IEEE 22nd International Conference on Communication Technology (ICCT), Nanjing, China, 2022, pp. 1437-1441.

[4] H.-L. Maattanen et al., "5G NR Communication over GEO or LEO Satellite Systems: 3GPP RAN Higher Layer Standardization Aspects," 2019 IEEE Global Communications Conference, pp. 1-6, 2019.

[5] 3GPP, "TS 23.501 V16.1.0; System Architecture for the 5G System," Jun. 2019.

[6] A. Maeder et.al., "Towards an Architecture Vision for Beyond 5G," 6G Conference, Levi, Finland, Mar. 2019.

[7] B. Bertenyi, "5G Standardization update," 3GPP Webinar, Jul. 2019. Online. Available: https://www.3gpp.org/news-events/2058-ran-rel-16-progress-and-rel-17-potential-work-areas, Aug. 3, 2019.

[8] X. Jing, H. Wang, F. You, Y. Wei, L. Chen and Y. Yang, "A Comparison of SSPA and TWTA for Beidou Navigation Satellite System," 2021 International Conference on Microwave and Millimeter Wave Technology (ICMMT), Nanjing, China, 2021, pp. 1-3.

[9] E. K. Mensah, T. A. Ashitei and J. K. Arthur, "Linearization of High Power Amplifier Using A Memristor in Microwave Transmission," 2019 International Conference on Communications, Signal Processing and Networks (ICCSPN), Accra, Ghana, 2019, pp. 1-7.

[10] K. Singh, M. R. Bharti and S. Jamwal, "A modified PAPR reduction scheme based on SLM and PTS techniques," International Conference on Signal Processing, Computing and Control, Solan, 2012, pp. 1-6.

[11] B. M. Kang, H. -G. Ryu and S. B. Ryu, "A PAPR Reduction Method using New ACE (Active Constellation Extension) with Higher Level Constellation," 2007 IEEE International Conference on Signal Processing and Communications, Dubai, United Arab Emirates, 2007, pp. 724-727.

[12] Sairam Vamsi, T., Terlapu, S.K., Vamshi Krishna, M. (2022). PAPR Analysis of FBMC and UFMC for 5G Cellular Communications. In: Satapathy, S.C., Peer, P., Tang, J., Bhateja, V., Ghosh, A. (eds) Intelligent Data Engineering and Analytics. Smart Innovation, Systems and Technologies, vol 266. Springer, Singapore.

[13] Maheswari, M., Nagarajan, N.R., Banupriya, M. (2020). "Performance Analysis of UFMC System with Different Prototype Filters for 5G Communication," International Conference on Artificial Intelligence, Smart Grid and Smart City Applications. AISGSC 2019.

[14] Zhang Jian feng, Cheng Jian, Liu Bo and Yue Qiang, "Performance comparison of phase modulated system based on DSSS with HPA nonlinearity," IEEE International Conference on Wireless Communications, Networking and Information Security, Beijing, 2010, pp. 13-17.

[15] Anderson J A. "An Introduction to Neural Networks," MIT Press, Cambridge, 1995.

[16] M. k. Alsmadi, K. B. Omar, S. A. Noah and I. Almarashdah, "Performance Comparison of Multi-layer Perceptron (Back Propagation, Delta Rule and Perceptron) algorithms in Neural Networks," 2009 IEEE International Advance Computing Conference, Patiala, India, 2009, pp. 296-299.

[17] A. Ranganathan, "The Levenberg-Marquardt Algorithm," Honda Research Institute USA, 8 June 2004, Retrieved 12 August 2012.

[18] A. Kuh, "Mean squared error analysis of analog neural networks subject to drifting targets and noise," Conference Record of Thirty-Second Asilomar Conference on Signals, Systems and Computers (Cat. No.98CH36284), Pacific Grove, CA, USA, 1998, pp. 683-684 vol.1.

[19] P. Händel, "Understanding Normalized Mean Squared Error in Power Amplifier Linearization," in IEEE Microwave and Wireless Components Letters, vol. 28, no. 11, pp. 1047-1049, Nov. 2018.

[20] R. Schmogrow et al., "Error Vector Magnitude as a Performance Measure for Advanced Modulation Formats," in IEEE Photonics Technology Letters, vol. 24, no. 1, pp. 61-63, Jan.1, 2012.

[21] Fu-Ling Lin, Shin-Fu Chen, Liang-Fang Chen and Huey-Ru Chuang, "Computer simulation and measurement of error vector magnitude (EVM) and adjacent-channel power ratio (ACPR) for digital wireless communication RF power amplifiers," IEEE VTS 50th Vehicular Technology Conference, Amsterdam, 1999, pp. 2024-2028 vol.4.